

# Full Valence Band Photoemission from Liquid Water Using EUV Synchrotron Radiation

B. Winter,<sup>\*,†</sup> R. Weber,<sup>†</sup> W. Widdra,<sup>†,‡</sup> M. Dittmar,<sup>§</sup> M. Faubel,<sup>§</sup> and I. V. Hertel<sup>†,||</sup>

Max-Born-Institut für Nichtlineare Optik und Kurzzeitspektroskopie, Max-Born-Straße 2A, D-12489 Berlin, Germany, and Max-Planck-Institut für Strömungsforschung, Bunsenstr. 10, D-37073 Göttingen, Germany

Received: February 27, 2003; In Final Form: November 5, 2003

The valence band photoelectron spectra of liquid water (H<sub>2</sub>O and D<sub>2</sub>O) are studied in the photon energy range from  $h\nu = 60$  to 120 eV. The experiments use a 6  $\mu\text{m}$  diameter liquid-jet free vacuum surface at the MBI undulator beamline of the synchrotron radiation facility BESSY. Photoelectron emission from all four valence molecular orbitals (MOs) is observed. In comparison to those of the gas phase, the peaks are significantly broadened and shifted to lower binding energies by about 1.5 eV. This is attributed primarily to the electronic polarization of the solvent molecules around an ionized water molecule. Energy shifts, peak broadening, and relative peak intensities for the four MOs differ because of their specific participation in the hydrogen bonding in liquid water. Relative photoionization cross sections for MOs were measured for  $h\nu = 60, 80,$  and 100 eV. The main difference for liquid water, as compared to the gas phase, is the relative intensity decrease of the  $1b_2$  and  $3a_1$  orbitals, reflecting changes of the MOs due to H-bonding.

## I. Introduction

Liquid water, essential for all life processes, and its peculiar behavior make this molecule subject to intense and continuing research. The key to many properties of liquid water is hydrogen bonding (H-bonding). H-bonding in water can influence chemical processes. For instance, the formation of an O–H $\cdots$ O hydrogen bond weakens the O–H chemical bond, thereby enabling proton transfer via an exchange of these bonds.<sup>1</sup> Despite the importance of H-bonding, there are many unanswered questions, such as how H-bonding affects the electronic structure of pure water. At the same time, although H-bonding governs solvation it is still one of the most poorly understood interactions in chemical physics.

The present work focuses on the electronic structure of liquid water inferred from photoelectron emission using synchrotron light. For a long time, this technique was hardly applicable to highly volatile liquids because of the difficulty in transferring photoelectrons originating from the liquid surface through the vapor phase to an electron detector. This incompatibility of wet samples and ultrahigh vacuum has imposed serious limitations on accessing the electronic structure of liquids, although the ionization threshold energy of liquid water was reported some 20 years ago<sup>2</sup> to be 10.06 eV. Most recent experimental approaches have made use of X-ray absorption spectroscopy (XAS)<sup>3</sup>, X-ray Raman scattering (XRS),<sup>4</sup> and X-ray emission<sup>5</sup> to study the electronic structure of liquid water and water clusters.<sup>6</sup> In the XAS spectrum near the O 1s absorption edge, the pronounced structure characteristic for the free water molecule was found to be drastically smoothed and shifted toward higher energies in the liquid. Supported by ab initio calculations, this was attributed to a significant fraction of broken H-bonds with an average number of H bonds below

three.<sup>3</sup> The X-ray emission data also show a distinctive shift and broadening of the spectral features as a fingerprint of different broken H-bond configurations;<sup>5</sup> conclusions were similar to those found with XAS. Important complementary information on the structure of liquid water is obtained from X-ray diffraction (see, for example, refs 7 and 8 and the corresponding theory<sup>9,10</sup>), but the electronic structure is not directly addressed in this type of study.

To date, the only photoelectron emission study from valence levels in liquid water extending beyond the top of the valence band was performed with focused HeI radiation using a similar microjet setup to that in the present work.<sup>11,12</sup> With this laboratory photon source, the outer three valence orbital energies of liquid water were identified for the first time. However, because of the large background of secondary electrons in the spectra and limited statistics, peak positions and widths could not be determined precisely. In contrast, in the present work the microjet apparatus was modified for use at a synchrotron radiation source. When compared to the low-energy HeI photons, tunable undulator radiation is superior for a number of reasons: the much broader range of photon energies makes all valence electrons addressable to photoelectron spectroscopy, and the high brilliance allows us to accumulate high-resolution data with sufficient statistics. At the same time, the variation of the kinetic energy of the emitted electrons allows us in principle to access different depths below the surface and to carry out a systematic investigation of potential final-state effects, and the 100% polarization of the photons adds additional specificity to the experiment.

In the present work, we present the first full-range valence photoelectron emission spectra of liquid water obtained for photon energies up to 120 eV. This energy range enables the investigation of previously inaccessible electronic structural details and provides complementary information to recent X-ray studies.<sup>3,5</sup> We also report partial ionization cross sections  $d\sigma_i/d\Omega$  for all four liquid water molecule valence orbitals. The role of oriented surface species and the effect of H-bonding in the liquid on the electronic structure of the H<sub>2</sub>O molecule will be

\* Corresponding author. E-mail: bwinter@mbi-berlin.de.

<sup>†</sup> Max Born Institute.

<sup>‡</sup> Present address: Martin-Luther-Universität Halle-Wittenberg.

<sup>§</sup> Max-Planck-Institut für Strömungsforschung.

<sup>||</sup> Also at Freie Universität Berlin, Physics Department. URL: <http://staff.mbi-berlin.de/hertel>.

discussed. Finally, we identify inelastic scattering processes of the photoelectrons with the water molecules in the liquid.

## II. Experimental Section

A liquid, micrometer-sized water jet, 6  $\mu\text{m}$  in diameter, was generated in a high-vacuum environment. The small beam size results in nearly collisionless evaporation.<sup>13</sup>

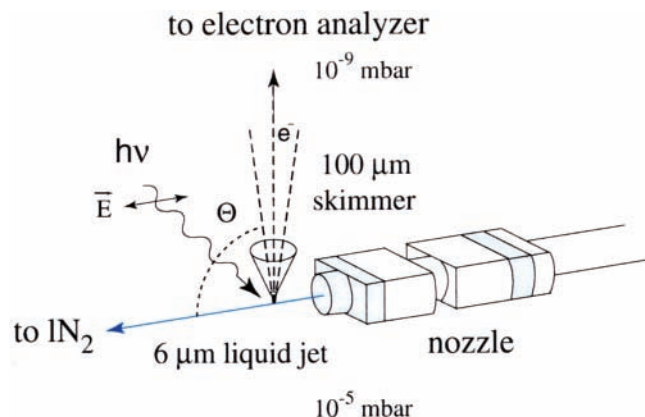


**Figure 1.** Schematic of the experimental setup. Polarization vector of the synchrotron light is perpendicular to the direction of the electron detection. Photoelectrons pass through the spectrometer skimmer, which acts as a differential pumping stage.  $\Theta$  is the emission angle with respect to the light polarization.

The photoemission measurements were performed at the MBI-BESSY undulator beamline (U125). It provides photon energies up to about 180 eV at an energy resolution of better than  $10^4$ . For the present experiments, the resolution was reduced in favor of the photoemission signal to about 100 meV, which is more than sufficient for the observed features with typical intrinsic widths of  $>0.5$  eV. At a photon flux of  $4 \times 10^{12}/\text{s}$  per 0.1 A ring current, count rates are on the order of 100 counts/s at the peak maximum. The synchrotron light intersects the laminar liquid jet at normal incidence, and electrons are detected normal to both the jet direction and the light-polarization vector (Figure 1). With a focal spot size of the synchrotron radiation of about 250  $\mu\text{m}$  along the jet and 120  $\mu\text{m}$  in width, the simultaneous detection of photoelectrons from gas-phase water surrounding the jet is unavoidable and even beneficial for calibration purpose, as we shall see.

The jet was thoroughly grounded to avoid charging upon photoemission, even though charging of the insulated surface is negligible for a flowing microsized system.<sup>11,12,14</sup> Highly demineralized water (conductivity ca. 0.2  $\mu\text{S}/\text{cm}$ ) was used in the experiments.

## III. Results and Discussion

**A. Liquid Photoemission and Reference Energy.** Figure 2 displays photoelectron spectra of liquid water obtained for 80, 100, and 120 eV excitation photon energy. The acquisition time per spectrum was 30–45 min. For clarity, the spectra are vertically displaced relative to each other, with the intensities being normalized to the  $1b_1$  (liquid) peak height.

Gas-phase contributions to our photoemission spectra result from the continuous evaporation of the liquid surface, and are indicated by the subscript g (e.g.,  $1b_{1g}$ ). The sharp feature corresponding to the  $1b_{1g}$  gas-phase  $\text{H}_2\text{O}$  orbital with its well-known binding energy of 12.60 eV<sup>15</sup> constitutes a precise energy reference. Its position and width are found to remain constant in our spectra as the jet was moved off-sight from the

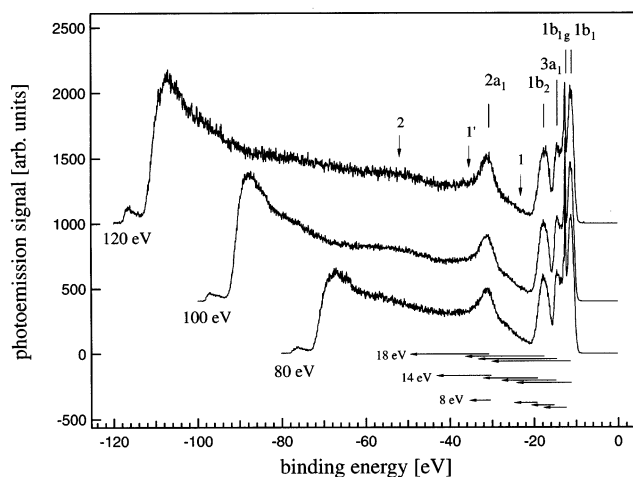


**Figure 2.** Full-range photoemission spectra from a 6  $\mu\text{m}$  diameter liquid water microjet obtained for 80, 100, and 120 eV photon energies, respectively. Peaks labeled  $1b_1$ ,  $3a_1$ ,  $1b_2$ , and  $2a_1$  correspond to the emission of the four water valence orbitals. Features 1,  $1'$ , and 2 are assigned to secondary processes involving electron energy losses due to quasi-optical excitation. Intensities are normalized to the  $1b_1$  (liquid) orbital energy. Electron binding energies are relative to vacuum. Transitions by optical absorptions, known for liquid water, are indicated by horizontal arrows.

spectrometer detection axis by about 100  $\mu\text{m}$ . Hence, all gas-phase water is sampled from a potential that is constant between the jet and the spectrometer skimmer, and binding energies reported here were calibrated to the  $1b_{1g}$  reference.

The 10–35 eV binding-energy region (Figure 2) is characterized by a clearly structured emission spectrum arising from the four valence orbitals of the  $\text{H}_2\text{O}$  molecule. Near 50 eV binding energy (label 2), broad emission features are observed. We will assign this structure, as well as some weaker features at lower binding energy (e.g., features 1 and  $1'$ ), to specific electron energy losses (section III E). This part of the spectrum also contains rather unspecific contributions from secondary electrons, giving rise to the broad background.

**B. Water Gas-to-Liquid Binding-Energy Shifts and Peak Broadening. 1. Overview of Experimental Findings.** The liquid- and gas-phase contributions to the spectra can be separated as illustrated in Figure 3, which shows the valence band photoemission spectra of water at  $h\nu = 60$  eV.

The top panel displays the measured liquid spectrum characterized by the maximum liquid-to-gas intensity ratio, from which a Shirley-type background was subtracted.<sup>16</sup> The center panel is the pure gas-phase spectrum. The labels in the figure denote the four (fully occupied) valence molecular orbitals (MOs) illustrated in Table 1) of the water molecule ( $C_{2v}$  symmetry) corresponding to the  $(1a_1)^2(2a_1)^2(1b_2)^2(3a_1)^2(1b_1)^2$  electronic ground-state configuration.<sup>17</sup>

The bottom curve in Figure 3 is the difference between the liquid and the gas-phase spectra (with properly scaled relative intensities of the  $1b_{1g}$  peak). This difference is our best experimental approach to the valence photoemission spectrum of pure liquid water. The most noticeable effect between the pure liquid and the gas-phase spectra is a binding-energy shift of all water orbitals to lower values, accompanied by considerable liquid peak broadening as summarized in Table 1. Any effect of the photon energy (60, 80, and 100 eV) on the electron binding energy and peak width is within the experimental error.

The energies given in Table 1 result from a Gaussian peak fitting averaged over a number of spectra. Figure 4 shows a representative example for  $h\nu = 60$  eV. As will be explained

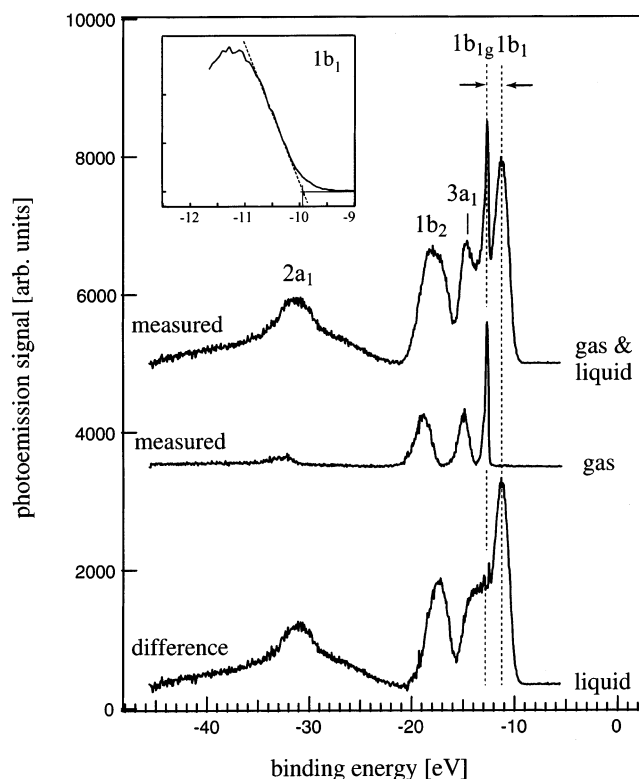


**Figure 3.** Photoemission spectra ( $h\nu = 60$  eV) from gas-phase water sampled for the maximum liquid signal (top), from the pure gas-phase 0.5 mm aside from the liquid microjet (center), and the difference spectrum (bottom). Labels refer to the four valence MOs of liquid  $1b_1$ ,  $3a_1$ ,  $1b_2$ ,  $2a_1$ . Also indicated is the prominent  $1b_{1g}$  gas-phase contribution. The gas-to-liquid binding-energy shift between  $1b_{1g}$  and  $1b_1$  is marked. Binding energies are with respect to vacuum. The inset shows the onset of the photoemission signal on an enlarged energy scale.

in section III E, the background underneath the  $2a_1$  signal was subtracted by fitting it to two energy-loss peaks. In contrast, as discussed in section III D, the  $3a_1$  signal itself was assumed to be split, the respective peak position given in Table 1 being an average of two single peaks and the width giving the overall energy spread of the two components. The statistical errors are indicated in Table 1.

The differential gas–liquid peak shifts for the four valence MOs given in Table 1 place the binding energy of the HOMO,  $1b_1$ , of liquid water at 11.16 eV (vertical transition energy), and the photoionization threshold of 9.9 eV is derived from extrapolating the slope of the  $1b_1$  signal (inset in Figure 3), which is slightly lower than that reported in the first threshold experiment.<sup>2</sup> It is interesting that recent photoelectron studies of water clusters<sup>6</sup> yield values for the shift and broadening between the free water molecule and the liquid. Note that the presently determined peak shifts are distinctively different from the values obtained earlier using HeI line radiation,<sup>11</sup> where 1.70, 1.35, and 1.59 eV for the  $1b_1$ ,  $3a_1$ , and  $1b_2$  orbitals, respectively, were reported. The differences are attributed to the considerably improved counting statistics and reduced secondary-electron background in the present experiment. Also, the earlier experiment was not capable of determining the peak widths, and the  $2a_1$  orbital was not accessible at all in these studies.

**2. Origin of Gas-to-Liquid Binding-Energy Shift.** The observed gas–liquid peak shifts of water are the net result of at least three different contributions: electronic polarization, surface dipoles, and changes in the orbitals due to H-bonding in the water network. We expect the first two contributions to be dominant and identical for all orbitals. The polarization term

accounts for the fact that the molecular electrons can be considered to move in an electric field that is screened by the polarization of the (liquid) environment around the molecular core. This is given by the relative permittivity  $\epsilon$  of the solvent. Because the emission process itself is very fast (femtosecond time scale), any reorientation of the solvent water molecules can be neglected, and the binding energy of the electrons is directly reflected in their kinetic energy after photoemission.<sup>17</sup> The observed shift on the order of 1–2 eV is common in the photoemission of condensed (molecular) systems. For liquids, this “polarization screening” may be estimated from the Gibbs free energy of solvation given by the Born equation<sup>17,25,26</sup>

$$\Delta G^{\text{Born}} = -\frac{z^2 e^2}{8\pi\epsilon_0 R} \left(1 - \frac{1}{\epsilon}\right) = E_g - E_{\text{aq}} \quad (1)$$





where  $E_{\text{aq}}$  and  $E_g$  denote the respective aqueous and gaseous binding energies. For photoemission, it is the optical macroscopic relative permittivity of water,  $\epsilon = \epsilon_{\text{opt}} \approx 1.8$ ,<sup>27</sup> that describes the screening of the solvent, and  $R$  is identified with the first maximum of the oxygen–oxygen radial distribution function<sup>28</sup> or with an effective (theoretical) solute cavity radius,  $R_{\text{eff}}$ . Using  $R_{\text{eff}} = 2.24$  Å,<sup>29</sup> one obtains  $-\Delta G = 1.4$  eV, which is in surprisingly good agreement with the shifts observed experimentally (Table 1). This is attributed to the small size of the water molecule because it allows for the assignment of a well-defined cavity radius.<sup>17</sup>

Clearly, a simple continuum model cannot reproduce structural details and completely neglects individual interactions between different water molecules. Also, as mentioned above, the mere existence of a surface is a potential source of orienting molecules. Thus, in principle surface dipoles have to be taken into account. A layer of oriented molecules at the water surface would lead to a spectral shift of all emission features due to a change in the work function. The magnitude of this surface potential for liquid water is, however, not well known, but it is likely to be some ten mV,<sup>30</sup> consistent with the permanent dipoles of water molecules nearly lying in the surface plane.<sup>31</sup> Electrochemical studies report a value of about 25 mV.<sup>32</sup> The case of water molecules on solid surfaces will be discussed in section III D.

The effect of the change in the dipole moment between the gas and condensed phases has been addressed explicitly in refs 9, 10, and 32. In fact, band-energy positions of liquid water are still the subject of continuing debate,<sup>35</sup> with the only consensus being the assignment of 10.06 eV below the vacuum level for the top of the valence band,<sup>35,36</sup> in good agreement with early reports<sup>2</sup> of about 10 eV and our present value of 9.9 eV. The photoionization threshold energy of liquid water has been discussed intensively,<sup>36–39</sup> often in the context of solvated electron formation (involving photolysis, single- and multiphoton processes). Autoionization and photoionization vs optical charge transfer or electron transfer is discussed in ref 38, and a thermodynamic consideration can be found in ref 36.

Finally, we expect a truly intrinsic orbital-energy shift due to H-bonding, which will be orbital-specific. The first detailed theoretical discussion of H<sub>2</sub>O molecular orbitals in the liquid phase has been reported in refs 9, 10, and 34, and direct experimental observations were published only very recently.<sup>3,5</sup> The X-ray absorption spectroscopy (XAS) studies revealed the presence of a considerable fraction of asymmetric configurations of the water molecules, for which the H-bond is strongly distorted or broken on the H-donating site of the molecule.<sup>3,4</sup> Likewise, electronic structural changes due to broken H-bonding

**TABLE 1: Experimental Electron Binding Energies, Full Widths, and Experimental Gas-to-Liquid Energy Shifts,  $E_g - E_{aq}$ , for the Four  $H_2O$  (Liquid and Gas) Valence Orbitals<sup>a</sup>**

orbital	binding energy/eV			peak width fwhm/eV			shift/eV
	gas	liquid	ice	gas	liquid	ice	gas-liquid
$1b_1$ 	12.60 <sup>15</sup>	11.16(4)	$\sim 12.3^{18,19}$ $\sim 11.8^{21}$	0.30(1)	1.45(8)	$\sim 1.3^{23}$ $\sim 1.28^{22}$	1.45(5)
$3a_1$ 	14.84(2) 14.80 <sup>15</sup>	13.50(10)	$\sim 14.2^{18,19}$	1.18(2)	2.42(10) <sub>22,23</sub> split	$\sim 2.5-3.0$	1.34(12)
$1b_2$ 	18.78(2) 18.60 <sup>15,24</sup>	17.34(4)	$\sim 17.6^{18,19}$ $\sim 18.0^{20}$	1.75(5)	2.28(8)	$\sim 2.0^{23}$ 1.82 <sup>22</sup>	1.46(6)
$2a_1$ 	32.62(10) 32.60 <sup>15</sup>	30.90(6)	$\sim 31.0^{21}$	2.82(14)	3.30(6)	$\sim 3.3^{21}$	1.72(16)

<sup>a</sup> The energy calibration is with respect to the  $1b_1$  gas-phase binding energy. The analysis is based on the Gaussian peak fitting of the respective difference spectra (liquid minus gas) obtained for 60, 80, and 100 eV photon energies, respectively. Data refer to the present work unless indicated otherwise. For comparison, we also report binding energies and peak widths for ice from the literature (fwhm being estimated also from literature data),

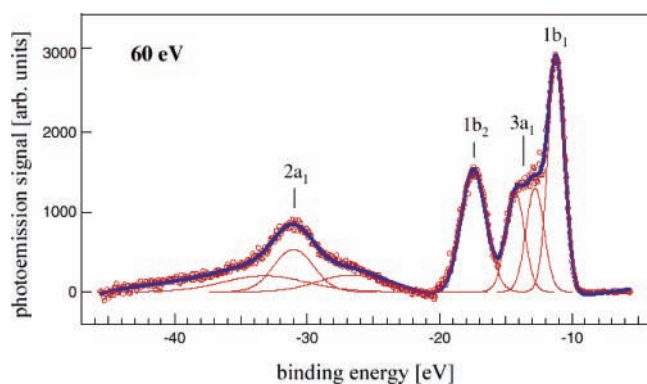


**Figure 4.** Representative Gaussian peak fitting shown for a photoemission spectrum of liquid water (difference spectrum;  $h\nu = 60$  eV). The extra peaks required for fitting the  $2a_1$  peak account for secondary processes of photoelectrons from other orbitals. A double-peak structure has been assumed for the  $3a_1$  feature for reasons explained in the text.

have been inferred from X-ray emission studies.<sup>5</sup> The main result is a peak broadening associated with an energy-level splitting, in particular, for the  $3a_1$  orbital, which is attributed to an increase in the dipole moment of liquid water<sup>9,10</sup> and subsequent polarization and hybridization of the orbital. As shown by ab initio molecular dynamics studies, the average O–H bond length in the liquid phase is significantly larger than in the isolated molecule.<sup>9,10</sup> The peak shifts observed in the present photoemission experiment reflect the various contributions mentioned, but it appears plausible that the most strongly bound  $2a_1$  orbital experiences this O–H stretch and charge redistribution most strongly, and shows the largest gas–liquid shift, as documented in Table 1. Clearly, photoemission has a high potential for probing, in principle, the binding energy of individual orbitals directly and is complementary to the X-ray techniques that are sensitive to differences in orbital energies. However, a detailed interpretation requires corresponding ab initio calculations that are currently underway in our group.

**3. Discussion of Liquid Peak Broadening.** The peak widths for all valence orbitals are substantially increased in comparison to those of the gas phase, as shown in Table 1. For comparison, the table also contains the respective widths for the gas-phase peaks as derived from the present spectra.<sup>24</sup> The liquid peak widths are about 4.0, 2.1, 1.3, and 1.2 times those in the gas phase for  $1b_1$ ,  $3a_1$ ,  $1b_2$ , and  $2a_1$ , respectively. These widths reflect the statistical distribution of different configurations

around an individual  $H_2O$  molecule (i.e., broken or unbroken hydrogen bonds, and the orientation of next neighbors). Also, local geometry differences of surface versus near-surface water molecules, located within the first few layers, may be important. It is interesting to note that surface water would closely resemble the D-ASYM broken, asymmetric H-bond structure proposed in ref 3.

The different peak widths show that H-bonding and configurational fluctuations have different effects on different  $H_2O$  orbitals, in agreement with ref 5. It appears plausible that the  $1b_1$  orbital, which is most weakly bound, would be particularly sensitive to such changes (from 0.3 to 1.45 eV) even though its absolute width is the smallest. A very similar value, 1.5 eV, for the width of the  $1b_1$  band in liquid water was observed by X-ray emission.<sup>5</sup> The small width is associated with the nonbonding character of this orbital. Apparently, the  $3a_1$  orbital is also very strongly affected; this was also observed in X-ray emission, attributed there to the influence of H-bonding on the character of the  $3a_1$  state showing the strongest energy-level splitting.<sup>5</sup> The broadening for  $1b_2$  and  $2a_1$  is considerably smaller. However, a pronounced influence of H-bonding on the  $1b_2$  orbital is derived from the respective cross sections discussed in the next section.

**C. Relative Photoionization Cross Sections.** Photoionization cross sections of liquid water, reported in the present work for the first time, may provide additional information about changes in the character of the MOs. The measured relative differential photoionization cross sections,  $d\sigma/d\Omega$ , are presented in Table 2 (top). Peak integrals (normalized to the  $1b_1$  peak height) at  $h\nu = 60, 80,$  and  $100$  eV are given for both liquid- and gas-phase water. (Presently, no attempt has been made to determine absolute photoionization cross sections.) The results were obtained by fitting each pure-liquid photoemission spectrum to Gaussians, as illustrated in Figure 4. No significant dependence on the photon energy is observed, indicating that final-state effects play, if any, only a minor role.

The errors indicated in Table 2 were inferred by comparing different fitting procedures. Comparatively large errors for the  $3a_1$  orbital arise from the strong spectral overlap with the  $1b_1$  peak. The value is determined with the largest uncertainty because of the substantial, unknown background arising from inelastic electron collisional processes (section III E). For reference, the corresponding gas-phase integrals are also displayed in the table. They can be determined more accurately

**TABLE 2: Relative Experimental Liquid- and Gas-Phase Intensities<sup>a</sup> for the Four H<sub>2</sub>O Valence MOs,<sup>b,c</sup> Gas-Phase Anisotropy Parameters  $\beta^{15}$  Used in Equation 3, and Derived Relative Partial Photoionization Cross Sections,  $\sigma_i$** 

orbital	Measured Relative $d\sigma/d\Omega$					
	liquid			gas phase		
	60 eV	80 eV	100 eV	60 eV	80 eV	100 eV
$1b_1$	1.00	1.00	1.00	1.00	1.00	1.00
$3a_1$	0.96(6)	0.99(6)	1.06(6)	1.16(3)	1.23(3)	1.12(3)
$1b_2$	0.79(3)	0.65(3)	0.72(3)	1.68(4)	1.67(4)	1.50(4)
$2a_1$	0.39(8)	0.35(8)	0.33(8)	0.41(10)	0.40(10)	0.36(10)
	$\beta$ (Anisotropy Parameter) <sup>d</sup>					
				gas phase		
				60 eV	80 eV	100 eV
$1b_1$				1.53	1.58	1.59
$3a_1$				1.35	1.50	1.55
$1b_2$				1.00	1.12	1.21
$2a_1$				1.56	1.66	1.71
	derived $\sigma$					
	liquid			gas phase		
	60 eV	80 eV	100 eV	60 eV	80 eV	100 eV
$1b_1$	1.00	1.00	1.00	1.00	1.00	1.00
$3a_1$	0.69	0.84	0.96	0.84	1.03	1.02
$1b_2$	0.39	0.36	0.41	0.79	0.80	0.78
$2a_1$	0.46	0.47	0.51	0.44	0.50	0.51

<sup>a</sup>  $d\sigma_i/d\Omega$  as measured. <sup>b</sup> At  $h\nu = 60, 80,$  and  $100$  eV. <sup>c</sup> Data are normalized to the  $1b_1$  intensity. <sup>d</sup> From Banna et al.<sup>15</sup> Values for 60 eV have been extrapolated.

because of both the strongly reduced background and the fact that the peaks do not overlap.

In Figure 5a, we present the relative photoemission intensities graphically. Cross-section changes with respect to the gas phase are particularly noticeable for the  $1b_2$  orbital (reduction of  $\sim 50\%$ ), but the  $3a_1$  peak decreases only by  $\sim 10\text{--}20\%$  and the  $2a_1$  signal is unchanged within the error limits. Apparently, the  $1b_2$  water orbital is most strongly influenced by its (liquid) environment, a behavior that in view of its geometry (Table 1) is most likely connected to its participation in H-bonding.

However, we now have to address the effect of molecular alignment on the photoelectron angular distribution. Photoionization cross-section measurements in the gas phase (statistically oriented molecules) are preferentially performed at the magic angle<sup>40</sup> because this allows to determine cross sections that are independent of the experimental geometry. However, from the measured quantity  $d\sigma_i/d\Omega$  obtained for a given geometry, the integrated cross sections (relative partial photoionization cross sections)  $\sigma_i$  may be calculated if the so-called (energy-dependent) anisotropy parameter  $\beta_i$  is known. For linear polarization, we have<sup>40,41</sup>

$$\frac{d\sigma_i}{d\Omega} = \frac{\sigma_i}{4\pi} \left( 1 + \left( \frac{\beta_i}{4} \right) (1 + 3P_1 \cos 2\Theta) \right) \quad (2)$$

with  $2 \geq \beta_i \geq -1$  and  $\Theta$  being the angle between the momentum vector of the ejected electron and the polarization vector of the incident photon beam.  $P_1$  is its degree of linear polarization. For the present experiment,  $P_1 = 1$  (synchrotron light is 100% horizontally polarized), and  $\Theta = 90^\circ$  so that

$$\sigma_i = 4\pi \frac{d\sigma_i}{d\Omega} \left( 1 - \frac{\beta_i}{2} \right)^{-1} \quad (3)$$

This allows us, in principle, to derive the relative photoionization

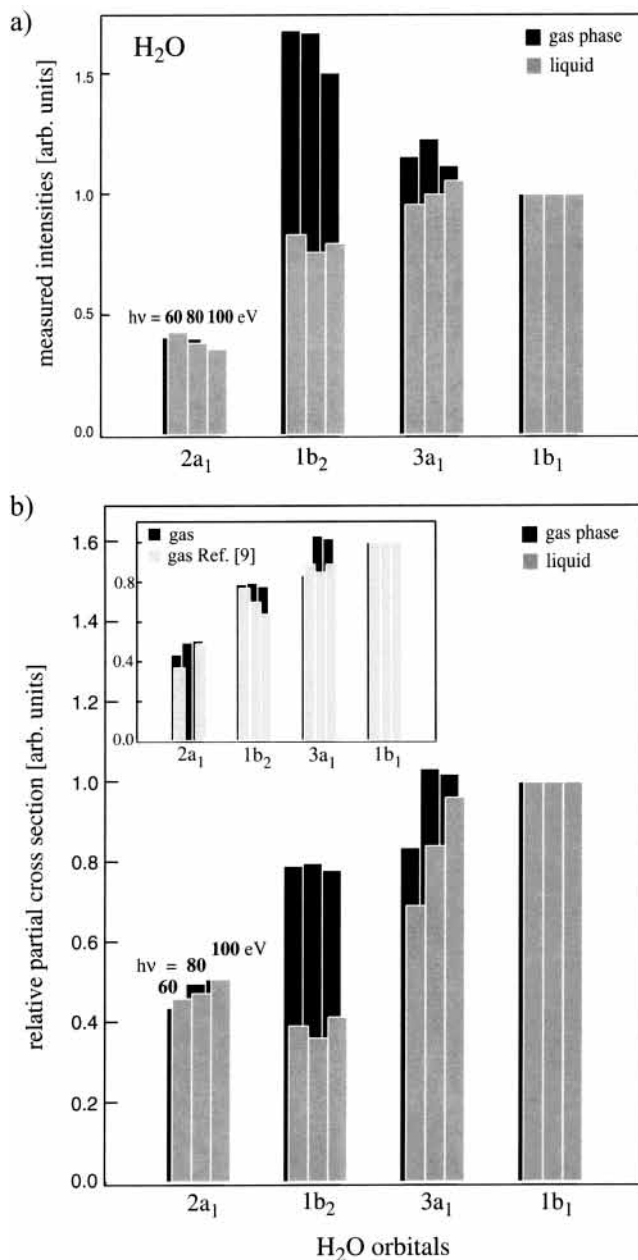


**Figure 5.** (a) Measured differential partial photoionization cross sections,  $d\sigma_i/d\Omega$  (Table 2), of the four H<sub>2</sub>O valence orbitals in the liquid and gas phases obtained for  $h\nu = 60, 80,$  and  $100$  eV. (b) Relative partial cross sections  $\sigma_i$  as derived from eq 3. Also shown is a comparison of gas-phase data from ref 15 (inset). All data are normalized to  $1b_1$  peak intensity.

cross sections for the different orbitals. Unfortunately,  $\beta_i$  parameters are known for gas-phase water only<sup>15</sup> (Table 2), and the present setup is not suited to determine  $\beta_i$  for the liquid phase. Consequently,  $\sigma_i$  can be calculated for the gas-phase spectra only. Our thus-derived gas-phase data  $\sigma_i$  agree well with those reported in ref 15. For comparison, Table 2 and Figure 5b also display  $\sigma_i$  for liquid water derived from eq 3 assuming  $\beta_i$  for the liquid and gas phases to be identical, which obviously leads to identical ratios between liquid- and gas-phase cross sections. However, in not knowing  $\beta_i$  for the liquid, one might also argue that the changes in the differential cross sections observed in the experiment (eq 2) are due to a decrease of the respective  $\beta_i$  parameters for the  $3a_1$  and the  $1b_2$  orbitals. One may even argue that the influence of the  $\beta_i$  parameter on the photoelectron signal could be more important because  $\beta_i$

depends not only on the amplitude but also on the phase shift of the outgoing partial electron waves. It was suggested that the reason for the comparatively small values of  $\beta_{1b_2}$  in the gas phase is related to the strong bonding character of this orbital.<sup>15</sup> H-bonding to neighboring molecules would strongly affect this behavior. However, in either case, a decrease of  $\sigma_i$  or  $\beta_i$  parameters, the behavior of the  $1b_2$  orbital (and, to a lesser extent, that of the  $3a_1$  orbital) is significantly different from that of the other MOs, and  $1b_2$  experiences the influence of the environment and H-bonding most strongly, unless we consider the unlikely case that all of the other orbitals change and the  $1b_2$  orbital is unaffected. This conclusion intuitively matches the orbital structures shown in Table 1. In contrast, the X-ray studies tend to indicate only a particular role of the  $3a_1$  orbital in the H-bonding.

Finally, we mention that we have also performed identical studies with deuterated water. Within the limits of the present experiment, the electronic structures of liquid H<sub>2</sub>O and D<sub>2</sub>O are indistinguishable. Neither the energetic positions nor the width and the relative cross sections of the two isotopomers show any measurable differences. This demonstrates, not completely unexpectedly, that no significant influence of zero-point vibrations can be observed under the present experimental conditions.

**D. Liquid Water versus the Ice Surface.** A direct comparison between the gas- and liquid-phase cross sections is, of course, justified only if there is no extra aligning mechanism for the latter case. Clearly, as mentioned above, a surface would exhibit some orientational order, and thus there is the possibility of surface-specific contributions to the cross-sectional behavior. This aspect is particularly important for the present photoemission experiment, which is highly surface-sensitive for photoelectron kinetic energies on the order of 20–120 eV as obtained here. Assuming that the electron mean-free path  $\lambda_e$  is similar for the solid and liquid phases, the information depth accessed for pure liquid water is about 2–4 water layers, which corresponds to about  $\lambda_e = 1$  nm assuming that the size of a water molecule is ca. 0.3 nm.<sup>26</sup> Experimental mean-free paths from liquid water have been reported for considerably lower kinetic energies only. The value obtained for 0.1–2.0 eV electrons, injected into water, is  $\lambda_e = 3$ –4 nm (or 10–15 monolayers of water),<sup>42</sup> and theory predicts values of about 3.5 nm for 1–20 eV in low-density amorphous ice.<sup>43</sup>

The liquid-water surface is assumed to be hydrogen-terminated with one free OH projecting into the vapor.<sup>31</sup> Also for adsorbed water, for instance, on a ruthenium single crystal, water molecules are thought to arrange in a bilayer.<sup>44</sup> Here, the higher-lying H<sub>2</sub>O molecules, which are not directly bound to the substrate, have one O–H bond oriented along the surface normal and contribute one H atom to the hydrogen-bonding network. In addition to this buckled icelike structure, a nearly flat first layer is obtained for Pt(111), where water molecules are adsorbed through alternating metal–oxygen and metal–hydrogen bonds.<sup>45</sup> Notice that for liquid water the OH axis pointing into the vacuum is likely to be more inclined toward the surface in order to stabilize the dipoles within the water–surface plane. Relative photoemission intensity differences of the outer valence band orbitals (i.e.,  $1b_1$ ,  $3a_1$ , and  $1b_2$ ) have indeed been observed for monolayer versus multilayer water adsorption.<sup>22,23,46,47</sup> This implies that the overall orientation of water molecules in the monolayer is different from that in the multilayer, consistent with the influence of surfaces in orienting water monolayers. A quantitative explanation of these intensity variations has not yet been reported.

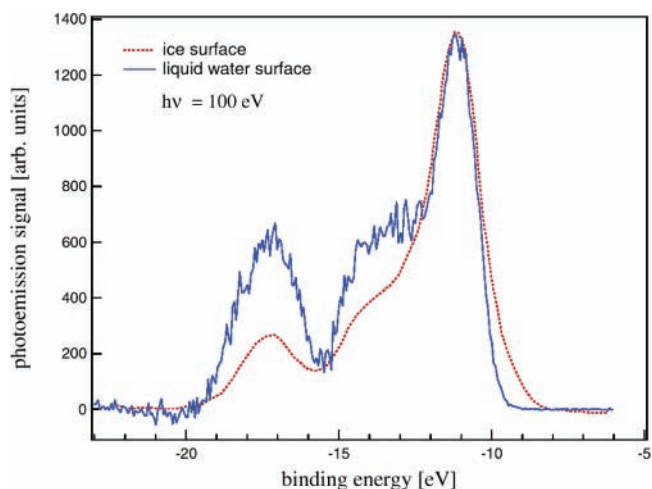


**Figure 6.** Photoemission spectra from 10-bilayer hexagonal ice grown on Pt(111) obtained for 75 eV photon energy (reproduced from Nordlund et al.<sup>22</sup>) and liquid water obtained for 80 eV. The ice spectrum was aligned by matching the  $1b_1$  peak position at the respective peak position of the liquid feature, which is 11.6 eV.

A striking common feature to all multilayer studies but also to results reported for solid ice is the relative intensity decrease of the  $3a_1$  orbital.<sup>19,23,46,47</sup> Generally, the multilayer spectra are almost identical irrespective of the surface used,<sup>18,46</sup> moreover, the multilayer spectra yield similar photoemission spectra to those found for liquid water in the present study.

This is illustrated in Figure 6, where we compare photoemission spectra from 10-bilayer hexagonal ice grown on Pt(111),<sup>22</sup> obtained for 75 eV excitation energy, with a photoelectron spectrum of liquid water measured at 80 eV. The spectra are normalized to the  $1b_1$  (liquid) peak height, and the binding energy axis of the ice spectrum was fixed with respect to the  $1b_1$  (liquid) binding energy. Clearly, whereas the overall shapes of the spectra are similar, the relative intensities of the photoemission from the different orbitals vary, with the ice showing even smaller intensities for the  $1b_2$  and  $3a_1$  orbitals, which is possibly an indication of more broken H bonds and/or differences in the surface structure. It should be noted at this point that the influence of surface species on the present photoemission results is not yet clear. Because the jet surface is curved, the radius being much smaller than both the synchrotron radiation focal size and the detector entrance of the spectrometer, the effective orientation of surface-water molecules varies, and any orientation-specific effect will almost average out. In addition, surface-orientation effects may be masked by the high mobility of the water molecules.

How similar are liquid water and solid ice with respect to their geometric and electronic structures? Both are governed by hydrogen bonding, and indeed the differences appear to be small (Table 1). Electron binding energies tend to be slightly larger in ice, by about 0.1–1.0 eV where the corresponding values obtained for adsorbed H<sub>2</sub>O multilayers on single-crystal surfaces<sup>19,22,23,46,47</sup> or for crystalline ice<sup>20,21</sup> are reported, and the widths for ice are based on a rather crude analysis of published spectra and do not show a significant difference to the liquid phase. The substantial band overlap of the  $3a_1$  and  $1b_1$  peaks and the  $3a_1$  peak splitting<sup>21,23</sup> further complicate such comparison. In a theoretical study of the electronic band structure of cubic ice, the splitting of the  $3a_1$  orbital was interpreted to arise from the Davydov interaction between two molecules of different orientation in the unit cell.<sup>3,47</sup> Electronic structural changes of the  $3a_1$  orbital, following the formation

of a surface, were also reported in a theoretical study of the surface properties of ice.<sup>49</sup>

**E. Electron Energy Losses in Liquid Water.** The presence of a pronounced and structured photoemission background in the liquid water photoelectron spectra that has no counterpart in the gas phase is a fingerprint of secondary interaction processes of the photoelectrons intrinsic to liquid water. High-energy (photo)electrons passing through the liquid medium excite the water molecules by inelastic collisions in a manner similar to photoexcitation.<sup>38,39</sup> For high-energy electrons, the selection rules are the same as for optical excitation (with forbidden transitions occurring at lower impact energies), and in the high-energy limit, the excitation probability is proportional to the optical dipole oscillator strength, which in turn is closely related to the energy-loss function,  $\text{Im}(-1/\epsilon(q, E))$ .<sup>39,50</sup> Hence, fast photoelectrons have a tendency to excite essentially the same states as white light and lose the corresponding energy. This is indeed what we observe in Figure 2. As compared to those of water vapor, the optical absorption bands are notably broadened, and the peak maxima are shifted to the blue.<sup>50–53</sup> In the absorption spectrum of liquid water,<sup>50,51</sup> maxima appear near 8, 10, 14, and 18 eV. Then, the loss structure near 50 eV (Figure 2, label 2) is interpreted to originate from  $2a_1$  photoelectrons exciting the 18 eV optical channel. One can attribute the wings (Figure 2, labels 1 and 1') of the native  $2a_1$  peak as well as the large width of the 50 eV feature to the respective energy losses associated with the lower-energy water orbitals. Specifically, the  $1b_2$ ,  $3a_1$ , and  $1b_1$  photoelectrons would make up for the shoulders in the  $2a_1$  region. Likewise, the 14 eV losses from initial  $2a_1$  photoelectrons are assumed to contribute to the low-binding-energy side of the 50 eV feature, extending up to ca. 54 eV. In ref 49, a strong maximum is found near 20 eV and a weaker maximum is found near 30 eV energy losses. Values for losses of <10 eV are smaller, by a factor of five and more, as compared to values at higher energies.<sup>49</sup> Qualitatively, the first loss maximum in  $\text{Im}(-1/\epsilon)$  would coincide with the occurrence of the 50 eV binding-energy feature in the present data (Figure 2), and possibly the second maximum with the weak feature near 82 eV.

#### IV. Conclusions and Summary

The valence photoemission peaks of liquid water,  $1b_1$ ,  $3a_1$ ,  $1b_2$ , and  $2a_1$ , are red-shifted and broadened as compared to those of gas-phase H<sub>2</sub>O. The energy shifts are attributed to the electronic polarization by the surrounding water molecules during the photoemission process. Differences in binding-energy shifts are assigned to changes in the water molecular orbital structure associated with H-bonding. The peak broadening largely reflects different local environments of water molecules in the liquid. In addition, a particularly strong reduction of the relative photoemission signal from  $1b_2$  in liquid water as compared to that from the gas phase indicates the specific sensitivity of this orbital to its environment, and most likely to changes in H-bonding. The observed peak shifts, broadening, and relative intensities of the H<sub>2</sub>O features were found to be independent of  $h\nu$  in the present range of photon energies (60 to 120 eV). Binding energies and widths presented in this study are significantly more precise than those obtained previously by excitation with HeI radiation.<sup>11,12</sup>

The photoemission spectra from liquid water were found to be similar to those of ice, with the  $3a_1$  peak being particularly broadened but even smaller intensities for the  $3a_1$  and  $1b_1$  peaks, either due to a different extent of broken H-bonds in the two phases<sup>3</sup> or to different surface structures. Finally, secondary

processes were identified where energy from fast photoelectrons is absorbed into the liquid, leading to the excitation of electronic states known from optical absorption spectroscopy.

In summary, photoelectron emission from a liquid microjet studied with synchrotron radiation has been shown to be possible and potentially a very sensitive tool for a detailed analysis of the electronic structure. Further studies and in particular ab initio model calculations are necessary to bring this to full fruition.

**Acknowledgment.** We acknowledge helpful discussions on this work with K. Godehusen and also A. Nilsson, who kindly allowed us to use his original data for the photoemission from ice for comparison. We thank N. Böwering and M. Wick for assistance with the experiment at its early stage, and R. Follath and G. Reichardt from BESSY for advising on beamline matters. The experiment was carried out at the CRG beamline of the MBI at BESSY in Berlin Adlershof.

#### References and Notes

- (1) Kropman, M. F.; Bakker, H. J. *J. Chem. Phys.* **2001**, *115*, 8942.
- (2) Delahay, P.; von Burg, K. *Chem. Phys. Lett.* **1981**, *83*, 250.
- (3) Myneni, S.; Luo, Y.; Naslund, L. A.; Cavalleri, M.; Ojamae, L.; Ogasawara, H.; Pelmenchikov, A.; Wernet, P.; Vaterlein, P.; Heske, C.; Hussain, Z.; Pettersson, L. G. M.; Nilsson, A. *J. Phys.: Condens. Matter* **2002**, *14*, L213.
- (4) Bergmann, U.; Wernet, P.; Glatzel, P.; Cavalleri, M.; Pettersson, L. G. M.; Nilsson, A.; Cramer, S. P. *Phys. Rev. B* **2002**, *66*, 092107.
- (5) Guo, J. H.; Luo, Y.; Augustsson, A.; Rubensson, J. E.; Sathe, C.; Agren, H.; Siegbahn, H.; Nordgren, J. *Phys. Rev. Lett.* **2002**, *89*, 13740.
- (6) Björneholm, O.; Federmann, F.; Kakar, S.; Möller, T. *J. Chem. Phys.* **1999**, *111*, 546.
- (7) Hura, G.; Russo, D.; Glaeser, R. M.; Head-Gordon, T.; Krack, M.; Parrinello, M. *Phys. Chem. Chem. Phys.* **2003**, *5*, 1981.
- (8) Krack, M.; Gambirasio, A.; Parrinello, M. *J. Chem. Phys.* **2002**, *117*, 9409.
- (9) Silvestrelli, P. L.; Parrinello, M. *J. Chem. Phys.* **1999**, *111*, 3572.
- (10) Silvestrelli, P. L.; Parrinello, M. *Phys. Rev. Lett.* **1999**, *82*, 5415.
- (11) Faubel, M.; Steiner, B.; Toennies, J. P. *J. Chem. Phys.* **1997**, *106*, 9013.
- (12) Faubel, M. Photoelectron Spectroscopy at Liquid Surfaces. In *Photoionization and Photodetachment*, part I; Ng, C. Y., Ed.; World Scientific: Singapore, 2000; p 634.
- (13) Faubel, M.; Kisters, T. *Nature* **1989**, *339*, 527.
- (14) Faubel, M.; Steiner, B.; Toennies, J. P. *J. Electron Spectrosc.* **1998**, *95*, 159.
- (15) Banna, M. S.; McQuaide, B. H.; Malutski, R.; Schmidt, V. *J. Chem. Phys.* **1986**, *84*, 4739.
- (16) Shirley, D. A. *Phys. Rev. B* **1972**, *5*, 4709.
- (17) Lundholm, M.; Siegbahn, H.; Holberg, S.; Arbmam, M. *J. Electron Spectrosc.* **1986**, *40*, 163.
- (18) Henderson, M. A. *Surf. Sci. Rep.* **2002**, *46*, 1.
- (19) Krischok, S.; Höft, O.; Günster, J.; Stultz, J.; Goodman, D. W.; Kempter, V. *Surf. Sci.* **2001**, *495*, 8.
- (20) Campbell, M. J.; Liesegang, J.; Riley, J. D.; Leckey, R. C. G.; Jenkin, J. G.; Pool, R. T. *J. Electron Spectrosc. Relat. Phenom.* **1979**, *15*, 83.
- (21) Shibaguchi, T.; Onuki, H.; Onaka, R. *J. Phys. Soc. Jpn.* **1977**, *42*, 152.
- (22) Nordlund, D.; Ogasawara, H.; Nilsson, A. *Maxlab Annual Report*; detailed data reported with permission by Nilsson, A.; 2001; p 236.
- (23) Peebles, D. E.; White, J. M. *Surf. Sci.* **1984**, *144*, 512.
- (24) Recent, independent gas-phase data (to be published) show significantly better agreement with the present data.
- (25) Born, M. *Z. Phys.* **1920**, *1*, 45.
- (26) Marcus, Y. *Chem. Rev.* **1988**, *88*, 1475.
- (27) Perry, J. H. *Chemical Engineers Handbook*; McGraw-Hill: New York, 1950.
- (28) Rick, S. W.; Stuart, S. J.; Berne, B. J. *J. Chem. Phys.* **1994**, *101*, 6141.
- (29) Bader, J. S.; Cortis, C. M.; Berne, B. J. *J. Chem. Phys.* **1997**, *106*, 2372.
- (30) Weber, R. Photoelectron Spectroscopy of Liquid Water and Aqueous Solutions in Free Microjets Using Synchrotron Radiation; Ph.D. thesis, Freie Universität Berlin, 2003.
- (31) Du, Q.; Superfine, R.; Freysz, E.; Shen, Y. R. *Phys. Rev. Lett.* **1993**, *70*, 2313.
- (32) Farrell, J. R.; McTigue, P. *J. Electroanal. Chem.* **1982**, *139*, 37.

- (33) Laasonen, K.; M, S.; Parrinello, M.; Car, R. *J. Chem. Phys.* **1993**, *99*, 9080.
- (34) Maw, S.; Sato, H.; Ten-no, S.; Hirata, F. *Chem. Phys. Lett.* **1997**, *276*, 20.
- (35) Coe, J.; Earhart, A. D.; Cohen, M. H.; Hoffmann, G.; Sarkas, H. W.; Bowen, K. H. *J. Chem. Phys.* **1997**, *107*, 6023.
- (36) Bernas, A.; Ferradini, C.; JayGerin, J. P. *Chem. Phys.* **1997**, *222*, 151.
- (37) Crowell, R. A.; Bartels, D. M. *J. Phys. Chem.* **1996**, *100*, 17940.
- (38) Sander, M. U.; Luther, K.; Troe, J. *Ber. Bunsen-Ges. Phys. Chem.* **1993**, *97*, 953.
- (39) Mozumder, A. *Phys. Chem. Chem. Phys.* **2002**, *4*, 1451.
- (40) Schmidt, V. *Electron Spectrometry of Atoms Using Synchrotron Radiation*; University Press: Cambridge, England, 1997.
- (41) Cooper, J.; Zare, R. N. *J. Chem. Phys.* **1968**, *48*, 942.
- (42) Neff, N.; Sass, J. K.; Lewerenz, H. J.; Ibach, H. *J. Chem. Phys.* **1980**, *84*, 1135.
- (43) Michaud, M.; Sanche, L. *Phys. Rev. A* **1987**, *36*, 4672.
- (44) Menzel, D. *Science* **2002**, *295*, 58.
- (45) Ogasawara, H.; Brena, B.; Nordlund, D.; Nyberg, M.; Pelmenchikov, A.; Pettersson, L. G. M.; Nilsson, A. *Phys. Rev. Lett.* **2002**, *89*, 276102.
- (46) Reissner, R.; Radke, U.; Schulze, M.; Umbach, E. *Surf. Sci.* **1998**, *402–404*, 71.
- (47) Bange, K.; Grider, D.; Sass, J. K. *Surf. Sci.* **1983**, *126*, 437.
- (48) We note here that for simplicity in all present data analyses we have assumed a double peak (of identical peak height and width) for the  $3a_1$  peak, consistent with Davydov splitting.
- (49) Casassa, S.; Ugliengo, P.; Pisani, C. *J. Chem. Phys.* **1997**, *106*, 8030.
- (50) Hayashi, H.; Watanabe, N.; Udagawa, Y.; Kao, C.-C. *J. Chem. Phys.* **1998**, *108*, 823.
- (51) Heller, J. M.; Hamm, R. N.; Birkhoff, R. D.; Painter, L. R. *J. Chem. Phys.* **1974**, *60*, 3483.
- (52) Gürtler, P.; Saile, V.; Koch, E. E. *Chem. Phys. Lett.* **1977**, *51*, 386.
- (53) Goddard, W. A.; Hunt, W. J. *Chem. Phys. Lett.* **1974**, *24*, 464.